Journal of Materials Chemistry A

Accepted Manuscript

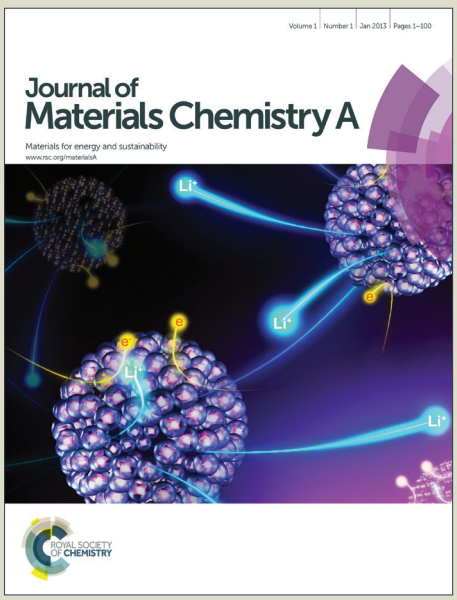

ROYAL SOCIETY OF CHEMISTRY

www.rsc.org/materialsA

Journal of Materials Chemistry A RSCPublishing

ARTICLE

Electrophoretic Deposition Improves Catalytic Performance of Co_3O_4 Nanoparticles for Oxygen Reduction/Oxygen Evolution Reactions

Cite this: DOI: 10.1039/x0xx00000x

Received 00th January 2012,
Accepted 00th January 2012

DOI: 10.1039/x0xx00000x

www.rsc.org/

M. Fayette,[a] A. Nelson[a] and R. D. Robinson[a b]

The effects of nanoparticle deposition on the catalytic activity of Co_3O_4 nanoparticles for the oxygen reduction reaction (ORR) and the oxygen evolution reaction (OER) are evaluated for two deposition methods: dropcasting and electrophoretic deposition (EPD). It is found that the EPD catalyst films demonstrate better catalytic activity per unit mass than do the dropcast films, as defined by diffusion-limited current, by about 27% for ORR and 25% for OER. When accounting for different loading levels, the absolute activities of these catalysts are superior to those of other reported Co_3O_4 colloidal nanoparticulate catalysts without conductive additives, showing that this material has excellent intrinsic activity for future optimization. Inspection of the electrode kinetics shows that EPD catalysts have more favorable characteristics as exhibited by their smaller Tafel slope (96 mV/decade for EPD versus 109 mV/decade for dropcast films). We analyze this enhancement by determining the metal oxide surface area for each catalyst film using a novel sequential metal deposition technique starting with electrodeposition of Ag followed by Pb underpotential deposition (UPD). Through UPD experiments we find, surprisingly, that EPD films have a smaller surface area than the dropcast films. We conclude that EPD films are more active per unit surface area. When accounting for surface area and mass, the EPD catalyst outperforms dropcast by a factor of 2.5 for ORR and 2.6 for OER. We anticipate that morphological differences in the EPD films relative to the dropcast ones, such as particle coverage and electrical conductivity, are responsible for this behavior. Such a result has important implications for future studies on the structure of EPD-manufactured nanoparticulate thin films and on the mechanisms for performance enhancement in such catalysts.

1. Introduction

The development of fuel cell materials has been of immense research interest for the past several decades. Specifically, the oxygen reduction (ORR) and oxygen evolution (OER) reactions have received much attention, with Pt[1-4] being the best metal catalyst. Both of these reactions are vigorously researched because they normally exhibit sluggish kinetics and high overpotential[1]. Researchers have tried to lower the amount of Pt needed in the fuel cell and to increase catalytic activity by exploring Pt-based thin film[5-13] and nanoparticle[14-17] (NP) catalysts such as PtPb[18-20], PtNi[21, 22], PtCu[14, 23-27], and PtRu[28-30]. The adoption of such catalysts, however, is hindered by the cost associated with Pt and other rare metals. Due to the high cost of Pt, other investigations have been focused on developing metal oxide catalysts, primarily based on Mn[31, 32], Fe[33-35], or Co[36-38] in alkaline solution. Co_3O_4[36, 39-45] coupled to nitrogen-reduced graphene oxide has been documented by Dai et al. as having comparable activity to Pt for ORR in addition to having extremely high OER activity.[39]

Regardless of the catalyst, dropcasting of the nanoparticles (NPs) onto the substrate surface is typically used, usually in conjunction with Nafion and some other conductive binder. Electrophoretic deposition (EPD) has recently been gaining attention as an alternative, possibly advantageous methodology for adhering NPs to substrates[44, 46-52]. Briefly, the EPD method involves the application of an electrical potential between two parallel conductive electrodes in a concentrated NP suspension. The electric field generated between the plates attracts the particles by the Coulombic force, since NPs typically have surface facets and defects associated with an intrinsic electric charge or a dipole moment that is not locally neutralized by stabilizing ligands. This method has been applied to Pt NPs[46-48], and we have previously shown the utility of this method for an additive-free (binderless and carbon-free) battery anode using Co_3O_4 NPs[51]. Binder-free systems represent a significant

advance since greater electrochemically active mass loadings are achievable within the same volume. Recently, Zheng et al.[53] showed that Pt NP films prepared by EPD have better ORR activity than those that are dropcast, but in this study the EPD process incorporated carbon nanofibers to enhance conductivity and used NPs of different sizes for each fabrication method, obfuscating a clear understanding of the results. To the best of our knowledge, no direct comparison for ORR/OER catalysis has been made between dropcast and EPD NP thin films fabricated using uniformly sized nanoparticles and without the use of conductivity enhancers.

In this work we critically compare dropcast thin films against EPD films of NP Co_3O_4 for ORR and OER. By using a binderless catalyst, we can clearly define the geometry of the conducting support. As a source for Co_3O_4, we use monodisperse epsilon Co (ε-Co) NPs. Previous work by our group indicates that the polycrystalline Co_3O_4 nanoparticles produced by oxidation of ε-Co have a high proportion of catalytically active (110) facets, promising improved activity[51, 54]. We have also previously shown that EPD can be used to manufacture mechanically stable films that have superior adhesion to the substrate; this feature is expected to improve performance. Furthermore, we use a more scalable "heat-up method" for NP synthesis to produce monodisperse ε-Co[55], in the hopes that such a process will allow future production of the pre-catalyst in quantity. Our work more stringently controls external factors by separating synthesis from catalyst deposition. Monodisperse particles (<10% size dispersion) are used. Previous work had poor control over the nanoparticle size distribution or did not attempt to control it, leaving the size-property relationships unclear. Our high-voltage EPD process allows us to deposit colloidal nanoparticles directly from an organic phase solution. Previous comparable work (see above) used EPD during particle synthesis[53], making the substrate-catalyst interaction even more difficult to understand. To electrochemically characterize the films we employ cyclic voltammetry (CV), linear sweep voltammetry (LSV), and chronoamperometry (CA). We use X-ray diffraction (XRD), transmission electron microscopy (TEM), and field emission scanning electron microscopy (FE-SEM) to characterize the phase and morphology of the NP catalysts. We find that the EPD NP catalyst films perform better than the dropcast films, as defined by diffusion-limited ORR and OER current per mass. Furthermore, the catalytic performance of these films for the ORR and OER is superior to other colloidal Co_3O_4 nanocatalysts reported previously. The kinetic characteristics of EPD films are also significantly improved compared to dropcast films, as can be seen from a reduced Tafel slope of 96 mV/decade vs. 109 mV/decade. This difference is significant, as previous research has shown even smaller Tafel slope differences are quite meaningful.[39] A reasonable assumption is that increased activity may be correlated with increased active surface area; to test this hypothesis, we explored a novel method for determining the metal oxide surface area for each catalyst film based on CA and CV of the reversible, sequential electrodeposition of Ag followed by Pb underpotential deposition (UPD) onto the films. Because UPD is highly specific (only occurring on noble metal surfaces) and intrinsically self-limiting (resulting in a coverage of one monolayer), it serves as an accurate tool for surface area measurements of suitable surfaces. We find dropcast films exhibit generally higher surface area than do EPD films, which is unexpected considering the higher mass-specific activity seen with EPD. As a corollary to this result, EPD films exhibit a greatly reduced surface area per mass; we attribute this to morphological differences between the films as a result of the different processes. The ultimate implication is that the morphology imposed by the EPD process must impart some other enhancement to the NPs or to the NP film to increase their activities.

2. Experimental

2.1 Synthetic procedures

Anhydrous 1,2-dichlorobenzene (DCB) (99%), tri-n-octylphosphine (TOPO) (99%), acetone (≥99.9%), anhydrous acetonitrile (≥99.8%), oleic acid (≥99%) and hexane (≥95%) were purchased from Sigma-Aldrich. Dicobalt octacarbonyl (stabilized 1-5% with hexane) was purchased from Strem. Anhydrous ethanol (200 proof) was purchased from KOPTEC. The TOPO was purified as described previously[56, 57]. We adapted synthetic procedures described previously[51, 54, 55, 58]. Standard Schlenk line techniques were used. The synthesis was conducted under an N_2 atmosphere. In a typical synthesis, 0.52 g of dicobalt octacarbonyl was mixed with 16 mL of 1,2-dichlorobenzene and 0.2 mL (approx. 0.36 g) oleic acid in a glove box under dry N_2. 0.1 g of purified TOPO was loaded into a 100 mL flask and degassed under vacuum to 200 mTorr three times. The solution of $Co_2(CO)_8$ and oleic acid in DCB was then added to the TOPO, and the resulting mixture was purged with N_2 for 15 minutes. The flask was then immersed in an oil bath heated to 195 °C, where the temperature of the solution was monitored by a K-type thermocouple. The solution was heated until the temperature was observed to drop (beginning at approximately 172-174 °C), after which it was held in the bath for 10 more minutes and then allowed to cool to room temperature. The product was extracted by mixing the solution 1:1 with ethanol, separating the product by centrifugation, re-suspending the precipitate in hexane, and repeating the process using excess acetone as the antisolvent. We note that complete extraction of all cobalt NPs is possible by diluting the solution to 2:1 ethanol:DCB as indicated by a purple supernatant presumably containing cobalt complexes after centrifugation, but the product obtained from this final process is polydisperse, containing significant amounts of very small particles. To eliminate polydispersity as a consideration, this complete extraction method was not used.

2.2 Preparation of glassy carbon (GC) electrodes

Glassy carbon disks with d = 0.5 cm and thickness = 4 mm were used as working electrodes (WE) in this study. The GC

was sequentially polished using water-based, 1 μm de-agglomerated alumina suspensions and 0.1 μm diamond suspension (Electron Microscopy Sciences), respectively. The GC was rinsed thoroughly with Direct-Q® water (>18 MΩ cm). The GC was then either used as polished or annealed at 450 °C for 1 hour in an oven open to air in order to improve adhesion[59].

2.3 Preparation of cobalt oxide catalysts

EPD of the Co NPs was conducted by immersing the GC electrode into a 1 mg/mL suspension of Co NPs in hexane. The cathode was a Pt wire. The GC was used as an anode with applied voltage of 300 V for 0.5 min using a high-voltage DC power source. Dropcasting of the particles was done by depositing the appropriate volume of the 1 mg/mL suspension to achieve the desired mass loadings. The catalyst was then annealed in a box oven at 230 °C for 2 hours in air in order to complete the conversion of Co to Co_3O_4 as demonstrated in our previous work[54].

2.4 Electrochemical testing and characterization

Prior to ORR/OER experiments, all catalysts were activated by cyclic voltammetry in the potential range of -0.4 V to -1.0 V in 0.1 M KOH (99.99%, Sigma-Aldrich) for 10 cycles, followed by 10 cycles from 0.6 to 0 V. Both steps were done after purging the cell with N_2 for 2 hours. ORR and OER experiments were conducted by LSV at 1600 RPM in O_2 saturated 0.1M KOH. Tafel analysis was conducted by analysis of ORR polarization curves at 1600 RPM, after mass-transport compensation of the current density[39, 60], where J, J_k, and J_L are the current density, kinetic current density, and diffusion limited current density, respectively: $J_k=(J\cdot J_L)/(J_L-J)$.

The electrochemical characterization of cobalt oxide was performed using a Bio-Logic VMP3 interfaced with a PC through the EC-Lab software (Version 10.36). All solutions were made using Direct-Q® water. Catalytic tests were done using a mercury oxide electrode (MMO) as the reference electrode and a Pt wire as the counter electrode.

2.5 Surface area analysis

EPD and dropcast catalysts were subjected to Ag deposition in 0.1 M $NaClO_4$ (99.99%, Sigma Aldrich) + 0.5 M NH_4OH (99.99% metals basis, Sigma Aldrich) + 0.002 M $AgClO_4$ (99.999% metals basis, Sigma Aldrich) at a constant potential of -1.35 V. After Ag deposition, Pb UPD was performed in 0.1 M $NaClO_4$ (99.99% Sigma Aldrich) + 0.01 M $HClO_4$ (99.99 % metals basis, Sigma Aldrich) + 0.003 M $Pb(ClO_4)_2$ (99.999% metals basis, Sigma Aldrich) by CV from -0.4 V to -0.81 V, followed by CA of UPD at -0.81 V for 10 seconds and of the reverse process at -0.5 V for 10 seconds. Potentials during deposition and stripping were referenced against the mercury-mercurous sulfate electrode (SSE) reference electrode with a Pt wire serving as the counter electrode. Finally, Ag dissolution was conducted in 0.1 M $NaClO_4$ + 0.5 M NH_4OH by LSV from -0.55 V to 0 V using an Ag^+/Ag pseudo-reference electrode. All solutions were made using Direct-Q® water.

2.6 EQCM analysis

EQCM measurements were performed with a model PM-700 Plating Monitor (Maxtek Inc.). The EQCM electrode, A = 1.37 cm^2, has a resonant frequency of f_0 = 5.000 MHz, density of ρ = 2.648 g cm^{-3}, and shear modulus of μ = 2.947x10^{11} g cm^{-1} s^{-2}. The sensitivity of the instrument[61] shows that a 1 Hz frequency change corresponds to a mass change of 24.2 ng (See Supporting Information).

2.7 Ex-situ surface characterization

TEM characterization of Co NP after synthesis was done using an FEI Tecnai F20 using an accelerating voltage of 120 kV. XRD characterization of the ε-Co and Co_3O_4 NPs in dry powder form was performed on a Scintag θ-θ diffractometer in θ-2θ configuration powder with a Ge-(Li) detector using Cu Kα radiation. SEM images were obtained using a LEO 1550 FE-SEM with an accelerating voltage of 10.00 kV and a working distance of 3-6 mm.

3. Results and Discussion

3.1 XRD and TEM Characterization of Co-based NP

Figure 1A and 1B shows TEM images of the Co NPs prior to oxidation and after. The average particle size is 10.7 nm ±1.0 nm (particle count N=300), which grows to 14.8 ± 1.3 nm (N=334) after oxidation. As shown in our previous work[54] and that of others (see section 2.1) the combination of TOPO and oleic acid is necessary to tightly control the particle morphology. Polydispersity is limited to less than 10%. XRD results (Fig. 1C) indicate the as-synthesized NPs are ε-cobalt phase with the main peaks at approximately 44, 47 and 49°.[62] XRD patterns of the oxidized NPs are highlighted with main peaks at 32, 38, 44, 59 and 66° (JCPDS 1-071-4921), indicating full transformation to Co_3O_4.

3.2 FE-SEM analysis of Co_3O_4 film morphology

FE-SEM images (Figure 2A-D) show high (A, B) and low (C, D) magnification SEM images of the EPD and dropcast thin films after the NPs are deposited on the annealed GC substrate and further annealed for 2 hrs. There are subtle differences in both the packing and overlap in the dropcast sample (Fig. 2B) compared to the EPD sample (Fig. 2A). The dropcast sample is evidently thick and formed from many layers of NPs, and cracks are also visible. On the macroscale, the dropcast film (Fig. 2D) is more prone to peeling and breaks in continuity, whereas the EPD film in nearly defect-free over the entirety of the image (Fig. 2C). No large cracks are apparent, so the thickness of the NP layer is not apparent for the EPD film. At low magnifications, the EPD film clearly forms a more conformal surface. This is not surprising, as we have previously

shown that EPD films are highly mechanically durable and well-adhered to the substrate: Scotch tape applied to their surfaces, for example, will remove virtually no material when peeled away, while dropcast films can be stripped off easily.[51]

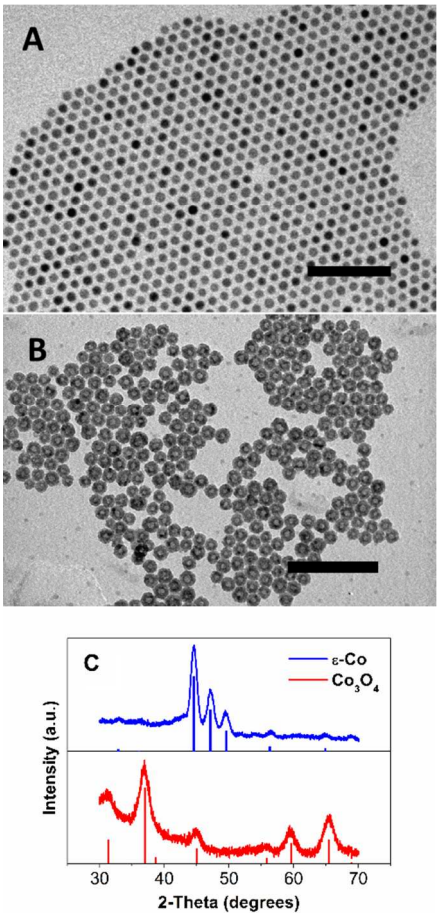

Figure 1: TEM image of Co NPs (A) prior to transformation to Co_3O_4 (B) and after oxidation. NPs are monodisperse spheres 10.7 ± 1.0 nm in diameter and grow to 14.8 ± 1.3 nm. Scale bars are 100 nm. (C) XRD of Co (blue) and Co_3O_4 (red) after chemical transformation. Index lines are from ref. 62 (ε-Co) and JCPDS #1-071-4921 (Co_3O_4).

3.3 EQCM assessment of EPD NP film mass loading

An electrochemical quartz crystal microbalance (EQCM) was employed to determine the mass of Co NPs deposited on the GC substrate. Figure 3 shows the results of the EQCM experiment. From 0-150 sec, the frequency is stable because the potential of 300 V has not been applied yet. At ~160 sec, the potential is applied and the frequency rapidly decreases to a value of ~-2600 Hz at ~190 sec and shows a constant oscillation of ~400-500 Hz. Although the rationale for this final oscillation event is currently unknown, one likely cause is that the outermost NPs fall off the electrode surface resulting in a frequency increase, while concurrently NPs are still depositing on the QCM surface, resulting in frequency decrease. The end result is a semi-steady state process where the mass is relatively uniform on the surface, indicating the EPD process results in no further accumulation of material. Of interest in the deposition of the Co NPs is that the frequency reaches this quasi-steady state after a relatively short deposition period (~50 seconds after potential is applied). Longer deposition times may result in the oxidation at the anode of both the substrate and particles, providing a rationale for a short deposition time. It should be noted that the conductor on the EQCM crystal is Au, not GC; however, we expect that deposition of the Co NPs should be similar in behaviour, as both are highly inert conductors. EPD does not result in a chemical reaction between the substrate and the NPs—before oxidation, the NPs may still be easily removed with hexane.

With the knowledge that the GC geometric surface area is 0.2 cm^2, a total of 9.2±2 µg of Co NPs are deposited by EPD in the 30 second time frame (see Supporting Information). In contrast to the relatively large deviation in mass measurement from the frequency oscillation, we found electrochemically (see next section) that the activity of the EPD catalyst was highly reproducible, thus justify our use of the average value as the reproducible EPD mass. As a comparison, many other catalytic experiments have a dropcast mass of NPs that is twice as high (20 µg).[33, 60]

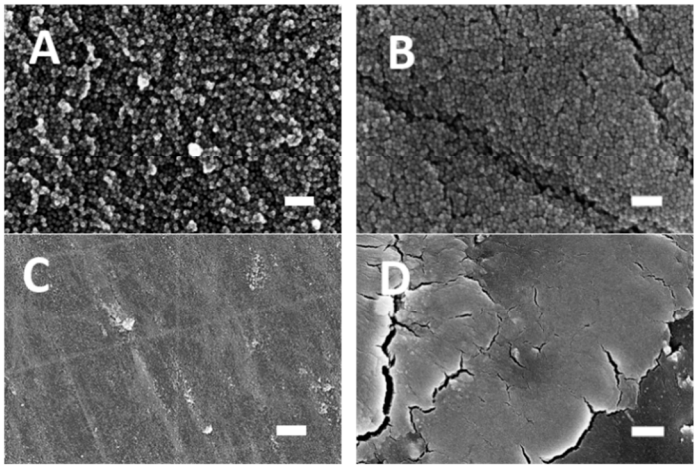

Figure 2: FE-SEM images at high and low magnification of (A, C) 30 sec EPD Co_3O_4 film (approximately 9.2 µg) and (B, D) 5 µg dropcast Co_3O_4 film. Scale bars are 100 nm (A, B) and 1 µm (C, D).

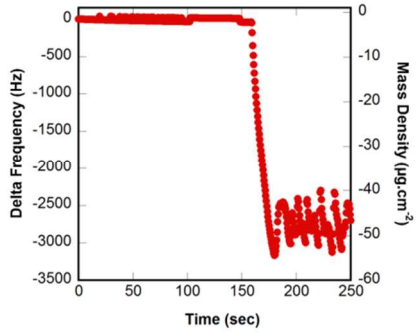

Figure 3: EQCM measurements for EPD of Co NPs. Solution: 1 mg/mL Co NP in hexane. Potential of 300 V is applied at time ~160 seconds.

3.4 Electrocatalytic evaluation of EPD and dropcast films

ORR is used as an electrochemical measure of the EPD and dropcast films' catalytic performance (Fig. 4A). In this work we focus mainly on the polarization curve analysis, as it best illustrates the results of our study; the determination of the pathway for ORR has previously been characterized to be predominantly 4e- in the case of Co_3O_4[39]. Three cases are compared: 5 µg of dropcast NPs, 10 µg of dropcast NPs, and EPD deposited particles (~9.2 µg as measured by EQCM) (Fig. 4A, green, blue, and pink curves, respectively). We have chosen to present all voltammetric curves as a function of current, rather than current density, because the electrochemically active surface area (ECASA)[15, 63] is not easily determined for non-noble metal catalysts (see section 3.5). Comparing the 5 µg dropcast and EPD, the EPD catalyst has a half-width potential $E_{1/2}$ of 0.299 V vs. -0.306 V for the 5 µg dropcast. At high overpotential (E<-0.3 V), these two samples have dissimilar diffusion limited current (-0.563 mA for the EPD catalyst versus -0.439 mA for the 5 µg dropcast catalyst). Considering that this is the same material but the EPD sample has higher loading, the difference between these $E_{1/2}$ and diffusion limited current values is not surprising; for films with microgram masses and lighter, one should expect the film with higher loading to perform better.[64, 65] Comparing the ~9.2 µg of Co_3O_4 from the EPD deposition versus the 10 µg from the dropcast deposition, the difference in $E_{1/2}$ is ~ -0.016 V, and the difference in the diffusion limited current is also relatively small (-0.563 mA for EPD vs. -0.493 mA for the 10 µg dropcast film). However, normalizing by mass and comparing the diffusion limited current, the ORR results show that EPD films have ~27% better catalytic properties than dropcast NP films of similar mass (-62.6 A/g vs -49.3 A/g for EPD and dropcast, respectively). In all cases, the current measurement is repeatable (to about 5%), well within the performance difference that we have established.

We evaluate the kinetics of the catalysts through Tafel analysis and find that the EPD catalyst is kinetically more active than a comparable dropcast catalyst. Figure 4B shows the Tafel plots for both EPD and dropcast catalysts. While differences in half-width potential and turn-on potentials are small, comparison of the Tafel slopes for ORR show significant differences: EPD films have a smaller slope of 96 mV/decade as opposed to 109 mV/decade for dropcast films (Figure 4B). A smaller slope is indicative of more favorable kinetic characteristics. These Tafel slopes are presented relative to the geometrical area of the substrate, rather than the areas of the catalysts that we determine later (see below). While better Co_3O_4 catalysts have been prepared using conductive supports (recent work reports much smaller Tafel slopes down to 37 mV/decade[39] for Co_3O_4 on nitrogen-doped reduced graphene oxide), our films exhibit similar activity (when corrected for the geometric area of the substrate) to that reported by Wang et. al. for nanoparticulate Co_3O_4 catalysts while using a mass loading roughly half of theirs[41] and our films also demonstrate comparable or superior activity to those prepared by Xu et. al.[40] and Xiao et. al.[42] despite our lower loadings and lack of conductive filler materials. In particular, our films show greatly enhanced activity compared to catalysts prepared by simpler thermal decomposition or hydrothermal methods,[39, 42] which shows that catalysts produced by our organic-phase synthetic approach have excellent potential. Furthermore, our observation of a smaller Tafel slope suggests that the kinetic characteristics have been significantly improved by the incorporation of a simple processing step (EPD).

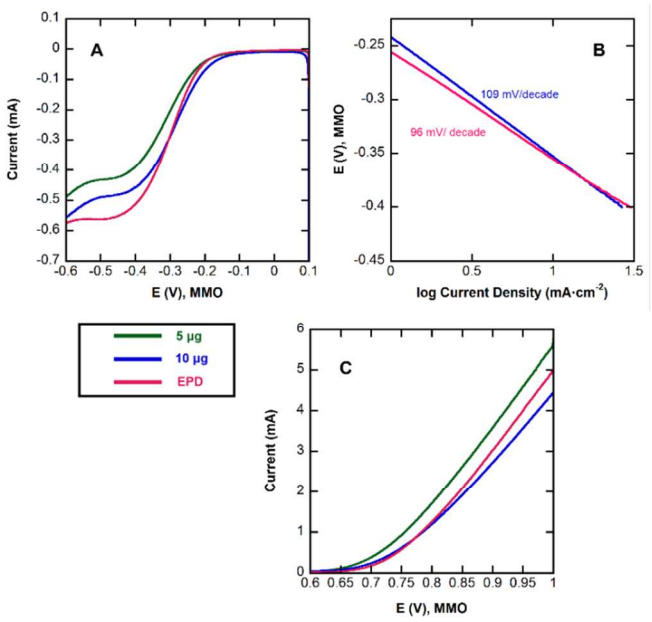

Figure 4: (A) ORR polarization curves for Co_3O_4 nanoparticle thin film deposited on GC by (pink) 30 seconds of EPD (~9.2 µg), (blue) dropcast of 10 µg, and (green) dropcast of 5 µg. (B) Tafel plots of 10 µg dropcast and EPD thin films derived by the mass-transport correction of corresponding RDE data. (C) OER polarization curves for (pink) 30 seconds EPD NP Co_3O_4 thin film, (blue) 10 µg Co_3O_4 thin film, and (green) 5 µg Co_3O_4 thin film on GC. Solution: 0.1 M KOH, O_2 saturated. Scan rate: 5 mV/s. Rotation speed: 1600 RPM.

To further investigate the performance differences in activity for EPD and dropcast catalysts, OER was examined (Fig. 4C). For OER the activity order is reversed from that of ORR: the 5 µg dropcast catalyst has an earlier turn-on potential (E=0.68 V) than the EPD catalyst (E=0.70 V). The 5 µg dropcast NPs has slightly higher activity at 1.0 V than the EPD (5.5 vs. 5.0 mA, respectively). However, when equal mass loadings are compared (10 µg dropcast vs. 9.2 µg EPD), the EPD catalyst outperforms the dropcast film activity at E= 1.0 V (5 mA vs. 4.5 mA for EPD and dropcast, respectively), with the turn on potential being the same. As a function of mass, the EPD outperforms the dropcast film activity by nearly 25% at E= 1.0 V (543 A/g vs. 450 A/g for EPD and dropcast, respectively). Compared to previous reports, our catalysts also exhibit comparable or higher activity, especially compared to unsupported catalysts[39, 41, 43]. This result confirms that the EPD

method for assembly of nanoparticle films produces highly active catalysts for the OER.

The results discussed above support a hypothesis that EPD forms nanoparticle films that have better interlinking between the particles and between the particles and the substrate. This improved connectivity leads to higher conductivity and faster charge transfer. These findings are consistent with our recent work that shows colloidal nanoparticle films assembled using EPD are denser and have higher electrically conductivity compared to films assembled through evaporative methods such as spin-casting, and also shows that the higher electrical conductivity is directly a result of enhanced interparticle connectivity from the EPD processing.[66]

While there is a remarkable difference in the Tafel slopes and diffusion-limited activities for both the EPD and dropcast thin films when freshly prepared, we focus only on comparisons of initial activity. Long term stability of these catalysts (not shown) for ORR is on the order of 24 hours under cycling conditions. For OER, the stability is greater than 80 hours in both cases. While previous stability testing has been done under constant potential conditions, we elected to cycle the potential at 50 mV/s during these time intervals between 0.1 and 0.8 V (vs. MMO) in order to demonstrate fuel cell/electrolyzer conditions (in which the potential might vary widely and repeatedly).

3.5 Electrochemical determination of Co_3O_4 surface area

In order to better understand the catalytic improvement seen in the EPD method, we undertook surface area evaluations of the nanocatalysts. Generally, for catalysis measurements involving Pt, the ECASA[15, 63] is determined by hydrogen UPD[67, 68] on the catalyst. For non-noble metals, the surface area is often determined by Brunauer–Emmett–Teller (BET) gas adsorption isotherms or the substrate geometric area is reported (not the true surface area of the catalyst). BET analysis can be difficult to employ with nanocatalysts, because BET requires a large quantity of material (~1 g) and elevated temperatures that can lead to coarsening of the material[69-72]. For our films (masses in the micrograms), it is not applicable. The use of geometric area of the substrate overestimates the catalytic activity since NP catalysts with typical loading (~20 μg[33, 60]) generally have surface areas of several cm^2 [15]. Many researchers employ substrates with geometric areas of ~0.2 cm^2, so the use of the geometric area overestimates the specific activity by a factor of 5, assuming an actual surface area of 1 cm^2. There have been attempts to determine electrochemically the area of Co_3O_4, such as the work by Trassati et al.[73]; however, this work attempted to determine the surface area by integration of the oxide formation charge, which at best yields an estimate of surface area within an order of magnitude.

To this end, we provide a preliminary methodology for electrochemically determining the surface area of the metal oxide NP films. Briefly, the method employs the following steps: (1) electrodeposition of Ag onto the NPs, which is monitored using CV and CA; followed by (2) Pb UPD onto the resultant Ag, which is monitored by using CV and CA. It has already been shown by Liu et al.[71] that Pb UPD can be employed to determine the surface area of nanoporous gold, and the proposed modification of this method for NPs should allow for a semi-quantitative determination of their surface area. The Ag layer is required because UPD occurs on noble metal surfaces.[74] Our group found in our previous work that all ligands were removed from Co_3O_4 NP surfaces following oxidation; at the same time, the particles could still be redispersed in solvent following the addition of new ligands, indicating that the particles had not been fused or sintered.[54] Therefore, the Ag should act as a thin conformal coating for the nanoparticle surfaces, upon which Pb UPD can occur for surface area analysis. Considering the discussion above and the results of Figure 2, there should be uniform Ag deposition onto the NPs, assuming the deposition is under mass-transport rather than charge-transfer conditions.

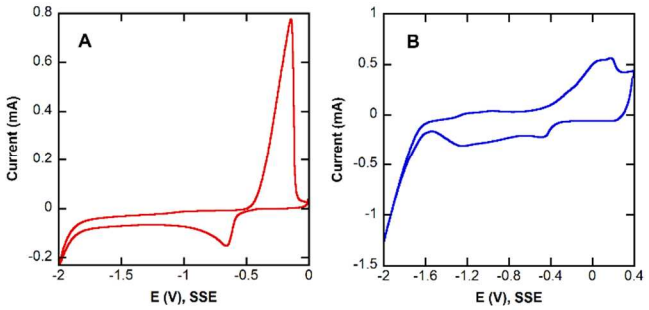

Figure 5: (A) Ag deposition CV curve on GC. (B) Ag deposition CV curve on EPD-formed Co_3O_4 thin film on GC. Solution: 0.1 M $NaClO_4$ + 0.5 M NH_4OH + 0.002 M $AgClO_4$, N_2 saturated. Scan rate: 100 mV/s.

Figure 5 shows the results of CV of Ag deposition in NH_4OH solution onto GC (Figure 5A) as a control to elucidate the deposition of Ag in the electrolyte and onto a Co_3O_4 thin film (Figure 5B) on GC. As in the catalytic measurements, use of a high pH solution is required, as Co_3O_4 is only stable in alkaline solution.[60, 75] While Ag deposition from alkaline solutions is usually performed in the presence of CN^-[76], ammonia was employed as a benign alternative, as it has been previously used for Ag deposition.[77, 78] The onset of Ag deposition occurs at -0.6 V while the main dissolution peak occurs at -0.3 V. The cathodic current starting at -1.9 V is due to hydrogen evolution on the surface. For Ag deposition/dissolution onto the cobalt oxide NPs, the CV features are more complex than that of the GC surface. During Ag electro-deposition, the applied potential for Ag deposition is usually slightly negative relative to the Ag reduction potential (e.g., -0.7 V for deposition vs. -0.6 V for Ag^+/Ag reduction onset). For Ag deposition onto cobalt oxide, the process is more complex. The formation of CoOOH and other cobalt oxides/hydroxides[60], as well as the more positive reduction potential of Ag compared to that of Co metal, necessitates that the applied potential be negative to the Co reduction potential (E = -1.25 V). The chosen potential must also stabilize the

surface against corrosion of Co^{+2} and Co^{+3} by NH_3[79] and take into account the shift of Co redox potentials to more negative values[80]. Figure 5B shows that hydrogen evolution on Co_3O_4 is shifted about 400 mV more positive than on GC, further limiting the overpotential window in which Ag can be reduced and the Co oxide NP surface can be stabilized without loss of current efficiency to hydrogen evolution. The Ag reduction peak at -0.6 V is not visible due to the high redox activity of the Co_3O_4, with the peaks at -0.8 and -1.2 V being redox changes to the oxide. A target amount of about 5 mC of Ag was employed to ensure full surface coverage on the electrode surface, which was verified by anodic stripping voltammetry (see Supporting Information and Figure S1).

Once the Ag is electrodeposited on the NP, Pb UPD is performed (Fig. 6). The Pb UPD voltammetry on the GC is indicative of polycrystalline Ag, as indicated by the three sets of peaks at ~-0.7 V[81]. The surface area is calculated by dividing the integrated UPD charge by the UPD charge density of 0.300 mC/cm^2 [Pb UPD layer charge on Ag(poly)][82]: $A = Q/Q_{ML}$, where Q is the average charge passed and Q_{ML} is the charge for one monolayer of Pb. This is a similar approach to that of Liu et al.[71] for the electrochemical surface area determination of nanoporous Au thin films. The surface area is calculated to be ~0.8±0.2 cm^2 for the EPD films, compared to 1.5±0.5 cm^2 for 5 µg and 1.7±1 cm^2 for 10 µg dropcast films (see Supporting Information, Table S1). The wide range in values for the dropcast films may be due to peeling effects/poor adhesion of the NP to the substrate, while the EPD based films on average are more consistent in their surface area measurements. The smaller variation in EPD film areas shows that EPD may be used to fabricate more reproducible films. Overall, we find that the surface area in the dropcast films to be roughly twice as large as the EPD films. This result is surprising, since the EPD films outperformed the dropcast film in terms of mass-normalized activity and kinetics. The EPD films were thus expected to possess more exposed catalytic surfaces.

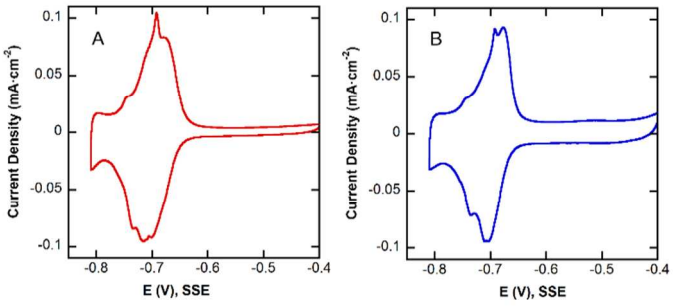

Figure 6: (A) Pb UPD on Ag film on GC. (B) Pb UPD on Ag film on EPD Co_3O_4 thin film. Solution: 0.1 M $NaClO_4$ + 0.01 M $HClO_4$ + 0.003 M $Pb(ClO_4)_2$. Scan rate: 20 mV/s.

Surface area measurements for dropcast films presented in this work lie within a large range (1-3 cm^2). Bromberg et al.[15] tabulated surface areas of ~4-5 cm^2 for Pt_4Cu NP of similar size scale (~8-9 nm), and conventional loading (~20 µg), based on hydrogen UPD.[67, 68] When considering the larger mass loading and generally higher specific area per mass for these smaller particles, we see that the surface areas for our dropcast particle films are generally smaller than those for previously reported surface area measurements on an equivalent scale (see Supporting Information), that is, the UPD method will "find" a much smaller fraction of the theoretical surface area of the NPs. The accuracy for UPD surface area determination is contingent on a number of factors, the first being homogeneity of the surface; as we have seen from our measurements of Ag coverage based on electrochemical stripping, this condition should be satisfied. In addition, if any exposed substrate is present, which in the case of dropcast films is a distinct possibility, deposition is more likely to occur on the NP than the substrate. Preferential deposition on the NPs is due to the several layers of NP being at least ~15 nm higher than the substrate (the NPs have a bare diameter of about 14.8 nm), which results in a higher local concentration of Ag^+ ions on the NP versus the bare substrate. Next, the species used in UPD must have access to the entire area of the catalyst. To assess this possibility we observed the films in SEM after Ag deposition and Pb UPD cycling. Figure 7A and 7B show FE-SEM micrographs of a 10 µg thin film after Ag deposition (Figure 7A) and after Pb UPD (Figure 7B). Particle shape is preserved through the cycling steps despite the deposition of Ag, and no obvious signs of surface roughness (e.g., dendritic Ag growth) are present on the NPs. Because our surface area results from UPD are lower than expected, a possible cause could be that Pb is not able to access the entire structure of the film. A possibility exists that "crosslinked" regions of silver have effectively passivated an unknown volume of the NP film, closing off sections of NP aggregates and lowering the effective area for UPD analysis. We were not able to locate a clearly defined region of crosslinked or welded NPs under SEM (Figure 7), but it is clear that that very little space remains between the particles after oxidation, when the particles increase in size by 38% and their ligands are removed (see Figure 2B). Our group has previous shown that these processing conditions create Co_3O_4 nanoparticle films where the nanoparticles are not welded together, as they can scraped off and redispersed in solvent.[54] Our group has also observed higher packing fractions in NP films from i) ligand removal with ammonium sulfide[83], ii) oxidation of cobalt nanoparticles into cobalt oxide and the concomitant removal of ligands, and iii) EPD processing of nanoparticles[66]. The closer packing of the particles effectively reduces the surface area, especially once they are coated with Ag.

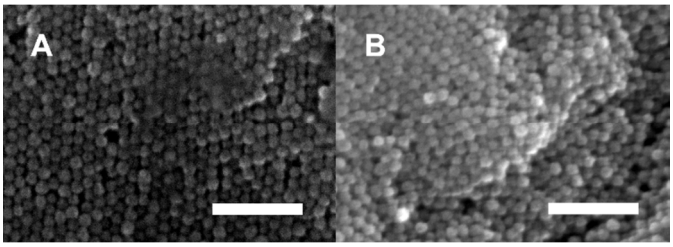

Figure 7: FE-SEM images of a 5 µg dropcast Co_3O_4 film (A) after Ag deposition and (B) after Pb UPD cycle. Scale bars are 100 nm.

Overall, since our UPD and dropcast UPD surface area measurements are performed identically, we conclude that the surface area of the dropcast film is approximately twice that of the EPD surface. Using a calculation to find surface area for various loadings, with the assumption that the NPs are spheres (see Supporting Information), we find the theoretical surface areas are larger than the experimental data by a factor of 5 (dropcast film measurements) to more than 10 (in the case of EPD films). The large difference between observed and calculated surface area is not surprising, however, in light of our previous observations that ligand removal, particle oxidation, and EPD all greatly increase particle connectivity and film density. Our results show that this method for surface area analysis clearly reflects morphological differences in the NP thin films. The rougher, less conformal appearance of dropcast films is consistent with the larger surface area measured using Pb UPD. Roughness in both films is observed, as the measured surface area considerably exceeds that of the substrate. Future work in this area will focus on optimizing the deposition steps, such as by electrodepositing a different metal (e.g., Pd) that is susceptible to hydrogen UPD, to allow the use of hydrogen UPD[15, 63, 68, 84] for surface area determination (the de facto standard for Pt group nanoparticles and surfaces). Since H is much smaller (Pb being ~3 times larger), this should allow for more accurate surface area analysis. Future work will also seek to quantify particle ordering and packing in the NP films.

Figures 8A and 8B show the results of the EPD and 10 µg dropcast films adjusted for the UPD calculated area. Considering the ORR and OER comparisons (Figure 4), these surface area results make the activity difference between EPD and dropcast more pronounced: for ORR, comparing the diffusion-limited current per actual surface area for the best case dropcast catalyst to the EPD catalyst, the EPD catalyst is ~2 times more active than the 10 µg dropcast thin film (Figure 8A). For OER the EPD catalyst is almost ~2 times more active than the 10 µg dropcast thin film (Figure 8B). If normalized to mass and surface area as in, the catalytic difference becomes a factor of >2.5 for ORR and ~2.6 for OER (Figure 8C and D).

4. Conclusions

Bifunctional thin film nanoparticulate catalysts for ORR and OER were synthesized by oxidizing ε-Co nanoparticles in air, forming Co_3O_4. The ε-Co nanoparticles were deposited by dropcasting and by EPD. In this study, we compare the catalytic activity of catalysts deposited by dropcasting to those deposited by EPD for the first time. Comparisons are made based on electrochemical activity, observations of morphology and mass loading in FESEM and EQCM, and a proof-of-concept surface area determination method based on depositing Ag onto the films followed by Pb UPD. Based on diffusion-limited current for ORR and current at 1.0 V vs. MMO for OER, normalized to mass, EPD films outperform those made by dropcasting by 27% for ORR and 25% for OER. When accounting for surface area and mass, the EPD catalyst outperforms dropcast by a factor of 2.5 for ORR and 2.6 for OER. In terms of absolute performance, our catalysts exhibit comparable or superior activity to several others reported previously. The area-specific performance for these catalysts produced by EPD as compared to catalysts deposited by dropcasting is enhanced, based on diffusion-limited current normalized to active surface area. EPD films are, surprisingly, more active per unit mass even though they appear to exhibit a smaller surface area. This performance increase for EPD is due to the morphological differences of the films: EPD films have previously been shown to be better adhered to the substrate and more mechanically stable under electrochemical conditions.[51] Thus, our work directly validates our hypothesis that EPD-prepared films have a better electrical connection to the substrate. Films produced by EPD exhibit better current conduction (accounting for better kinetic characteristics) and are denser, which is consistent with the previous findings of our group showing that EPD-prepared thin films have higher conductivity and better interparticle connections than those prepared through evaporative techniques such as spin-coating[66]. Further work should be done to confirm the applicability of the surface area determination method to a range of systems and to elucidate quantitatively the performance improvement in EPD.

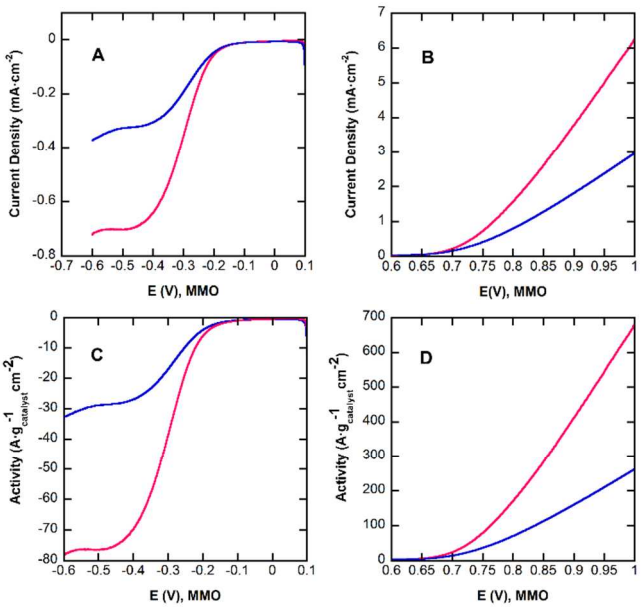

Figure 8: (A) ORR polarization curves for Co_3O_4 nanoparticle thin film deposited on GC by (pink) 30 seconds of EPD (~9.2 µg), and (blue) dropcast 10 µg after adjusting for surface area. (B) OER polarization curves for (pink) 30 seconds EPD Co_3O_4 thin film, and (blue) 10 µg Co_3O_4 thin film on GC after adjusting for surface area. (C) ORR polarization curves for Co_3O_4 nanoparticle thin film deposited on GC by (pink) 30 seconds of EPD (~9.2 µg), and (blue) dropcast 10 µg after adjusting for mass and surface area. (D) OER polarization curves for (pink) 30 seconds EPD Co_3O_4 thin film, and (blue) 10 µg

Co_3O_4 thin film on GC adjusting for mass and surface area. Solution: 0.1 M KOH, O_2 saturated. Scan rate: 5 mV/s. Rotation speed: 1600 RPM.

Acknowledgements

We thank the Héctor Abruña lab for use of their QCM and helpful discussions. This work was supported in part by the National Science Foundation (NSF) under award numbers CHE-1152922 and CMMI-1344562. This work made use of the Cornell Center for Materials Research Shared Facilities which are supported through the NSF MRSEC program (DMR-1120296). M.F. was partially supported as part of the Energy Materials Center at Cornell (EMC^2), an Energy Frontier Research Center funded by the U.S. Department of Energy, Office of Science, Office of Basic Energy Science under Award Number DE-SC0001086.

Notes and references

[a] Department of Materials Science and Engineering, Cornell University, Ithaca, NY 14853, USA.

[b] Author to whom correspondence should be addressed. Email: rdr82@cornell.edu

Electronic Supplementary Information (ESI) available: Calculations of EPD NP mass loading, Ag coverage and verification of Ag deposition, exact ranges of area determination, and detailed comparison with previous work by Bromberg.

1. N. M. Marković, T. J. Schmidt, V. Stamenković and P. N. Ross, *Fuel Cells*, 2001, **1**, 105-116.
2. R. R. Adzic, J. Zhang, K. Sasaki, M. B. Vukmirovic, M. Shao, J. X. Wang, A. U. Nilekar, M. Mavrikakis, J. A. Valerio and F. Uribe, *Top Catal*, 2007, **46**, 249-262.
3. E. Antolini, *Materials Chemistry and Physics*, 2003, **78**, 563-573.
4. V. Stamenkovic, N. M. Markovic and P. N. Ross Jr, *Journal of Electroanalytical Chemistry*, 2001, **500**, 44-51.
5. S. R. Brankovic, J. X. Wang and R. R. Adzic, *Surf Sci*, 2001, **474**, L173-L179.
6. J. Zhang, Y. Mo, M. B. Vukmirovic, R. Klie, K. Sasaki and R. R. Adzic, *J Phys Chem B*, 2004, **108**, 10955-10964.
7. J. Zhang, F. H. B. Lima, M. H. Shao, K. Sasaki, J. X. Wang, J. Hanson and R. R. Adzic, *J Phys Chem B*, 2005, **109**, 22701-22704.
8. M. F. Mrozek, Y. Xie and M. J. Weaver, *Analytical Chemistry*, 2001, **73**, 5953-5960.
9. K. Uosaki, S. Ye, H. Naohara, Y. Oda, T. Haba and T. Kondo, *The Journal of Physical Chemistry B*, 1997, **101**, 7566-7572.
10. T. Kondo, M. Shibata, N. Hayashi, H. Fukumitsu, T. Masuda, S. Takakusagi and K. Uosaki, *Electrochimica Acta*, 2010, **55**, 8302-8306.
11. D. A. McCurry, M. Kamundi, M. Fayette, F. Wafula and N. Dimitrov, *ACS Appl Mater Interfaces*, 2011, **3**, 4459-4468.
12. M. Fayette, Y. Liu, D. Bertrand, J. Nutariya, N. Vasiljevic and N. Dimitrov, *Langmuir : the ACS journal of surfaces and colloids*, 2011, **27**, 5650-5658.
13. J. Nutariya, M. Fayette, N. Dimitrov and N. Vasiljevic, *Electrochimica Acta*, 2013, **112**, 813-823.
14. D. Xu, S. Bliznakov, Z. Liu, J. Fang and N. Dimitrov, *Angew Chem Int Ed Engl*, 2010, **49**, 1282-1285.
15. L. Bromberg, M. Fayette, B. Martens, Z. P. Luo, Y. Wang, D. Xu, J. Zhang, J. Fang and N. Dimitrov, *Electrocatalysis*, 2013, **4**, 24-36.
16. S. Guo and S. Sun, *Journal of the American Chemical Society*, 2012, **134**, 2492-2495.
17. M. Oezaslan, F. Hasché and P. Strasser, *Journal of The Electrochemical Society*, 2012, **159**, B394-B405.
18. L. J. Zhang, Z. Y. Wang and D. G. Xia, *Journal of Alloys and Compounds*, 2006, **426**, 268-271.
19. N. De-los-Santos-Alvarez, L. R. Alden, R. E., F. J. Wang, F. J. DiSalvo and H. D. Abruna, *Journal of Electroanalytical Chemistry*, 2009, **626**, 14-22.
20. S.-M. Hwang, J. E. Bonevich, J. J. Kim and T. P. Moffat, *Journal of The Electrochemical Society*, 2011, **158**, D307.
21. V. R. Stamenkovic, B. Fowler, B. S. Mun, G. Wang, P. N. Ross, C. A. Lucas and N. M. Markovic, *Science*, 2007, **315**, 493-497.
22. Y. Liu, C. M. Hangarter, U. Bertocci and T. P. Moffat, *The Journal of Physical Chemistry C*, 2012, **116**, 7848-7862.
23. J. J. Mallett, U. Bertocci, J. E. Bonevich and T. P. Moffat, *Journal of The Electrochemical Society*, 2009, **156**, D531.
24. H. Yang, L. Dai, D. Xu, J. Fang and S. Zou, *Electrochimica Acta*, 2010, **55**, 8000-8004.
25. R. Yang, J. Leisch, P. Strasser and M. F. Toney, *Chemistry of Materials*, 2010, **22**, 4712-4720.
26. F. Hasche, M. Oezaslan and P. Strasser, *ChemCatChem*, 2011, **3**, 1805-1813.
27. M. Oezaslan and P. Strasser, *Journal of Power Sources*, 2011, **196**, 5240-5249.
28. J.-H. Choi, K.-J. Jeong, Y. Dong, J. Han, T.-H. Lim, J.-S. Lee and Y.-E. Sung, *Journal of Power Sources*, 2006, **163**, 71-75.
29. T. S. Mkwizu, M. K. Mathe and I. Cukrowski, *Langmuir : the ACS journal of surfaces and colloids*, 2009, **26**, 570-580.
30. N. M. Markovic, H. A. Gasteiger, P. N. R. Jr., X. Jiang, I. Villegas and M. J. Weaver, *Electrochimica Acta*, 1995, **40**, 91-98.
31. J. Ponce, J. L. Rehspringer, G. Poillerat and J. L. Gautier, *Electrochimica Acta*, 2001, **46**, 3373-3380.
32. K. L. Pickrahn, S. W. Park, Y. Gorlin, H.-B.-R. Lee, T. F. Jaramillo and S. F. Bent, *Advanced Energy Materials*, 2012, **2**, 1269-1277.
33. Z.-S. Wu, S. Yang, Y. Sun, K. Parvez, X. Feng and K. Müllen, *Journal of the American Chemical Society*, 2012, **134**, 9082-9085.
34. M. J. Bradley, A. J. Biacchi and R. E. Schaak, *Chemistry of Materials*, 2013, **25**, 1886-1892.
35. H. Zhu, S. Zhang, Y.-X. Huang, L. Wu and S. Sun, *Nano Letters*, 2013, **13**, 2947-2951.
36. M. De Koninck, S.-C. Poirier and B. Marsan, *Journal of The Electrochemical Society*, 2007, **154**, A381-A388.
37. R. Ning, J. Tian, A. M. Asiri, A. H. Qusti, A. O. Al-Youbi and X. Sun, *Langmuir : the ACS journal of surfaces and colloids*, 2013, **29**, 13146-13151.
38. S. Guo, S. Zhang, L. Wu and S. Sun, *Angewandte Chemie International Edition*, 2012, **51**, 11770-11773.

39. Y. Y. Liang, Y. G. Li, H. L. Wang, J. G. Zhou, J. Wang, T. Regier and H. J. Dai, *Nat Mater*, 2011, **10**, 780-786.
40. J. Xu, P. Gao and T. S. Zhao, *Energy & Environmental Science*, 2012, **5**, 5333-5339.
41. D. Wang, X. Chen, D. G. Evans and W. Yang, *Nanoscale*, 2013, **5**, 5312-5315.
42. J. W. Xiao, Q. Kuang, S. H. Yang, F. Xiao, S. Wang and L. Guo, *Sci Rep*, 2013, **3**.
43. Y. J. Sa, K. Kwon, J. Y. Cheon, F. Kleitz and S. H. Joo, *Journal of Materials Chemistry A*, 2013, **1**, 9992-10001.
44. B. H. R. Suryanto, X. Lu and C. Zhao, *Journal of Materials Chemistry A*, 2013, **1**, 12726-12731.
45. X. Lu and C. Zhao, *Journal of Materials Chemistry A*, 2013, **1**, 12053-12059.
46. T. Teranishi, M. Hosoe, T. Tanaka and M. Miyake, *The Journal of Physical Chemistry B*, 1999, **103**, 3818-3827.
47. H. Morikawa, N. Tsuihiji, T. Mitsui and K. Kanamura, *Journal of The Electrochemical Society*, 2004, **151**, A1733-A1737.
48. H. Munakata, T. Ishida and K. Kanamura, *Journal of The Electrochemical Society*, 2007, **154**, B1368-B1372.
49. M. A. Islam, Y. Xia, D. A. Telesca, M. L. Steigerwald and I. P. Herman, *Chemistry of Materials*, 2003, **16**, 49-54.
50. J. Dickerson, in *Electrophoretic Deposition of Nanomaterials*, eds. J. H. Dickerson and A. R. Boccaccini, Springer New York, 2012, ch. 3, pp. 131-155.
51. D. H. Ha, M. A. Islam and R. D. Robinson, *Nano Letters*, 2012, **12**, 5122-5130.
52. L. Besra and M. Liu, *Progress in Materials Science*, 2007, **52**, 1-61.
53. J.-S. Zheng, M.-X. Wang, X.-S. Zhang, Y.-X. Wu, P. Li, X.-G. Zhou and W.-K. Yuan, *Journal of Power Sources*, 2008, **175**, 211-216.
54. D.-H. Ha, L. M. Moreau, S. Honrao, R. G. Hennig and R. D. Robinson, *The Journal of Physical Chemistry C*, 2013, 130606160139003.
55. J. V. I. Timonen, E. T. Seppälä, O. Ikkala and R. H. A. Ras, *Angewandte Chemie International Edition*, 2011, **50**, 2080-2084.
56. H. Zhang, D.-H. Ha, R. Hovden, L. F. Kourkoutis and R. D. Robinson, *Nano Letters*, 2010, **11**, 188-197.
57. F. D. Wang, R. Tang and W. E. Buhro, *Nano Letters*, 2008, **8**, 3521-3524.
58. V. F. Puntes, K. M. Krishnan and A. P. Alivisatos, *Science*, 2001, **291**, 2115-2117.
59. Y. Gorlin, C.-J. Chung, D. Nordlund, B. M. Clemens and T. F. Jaramillo, *ACS Catalysis*, 2012, **2**, 2687-2694.
60. Y. Liang, H. Wang, P. Diao, W. Chang, G. Hong, Y. Li, M. Gong, L. Xie, J. Zhou, J. Wang, T. Z. Regier, F. Wei and H. Dai, *Journal of the American Chemical Society*, 2012, **134**, 15849-15857.
61. G. Sauerbrey, *Z. Physik*, 1959, **155**, 206-222.
62. D. P. Dinega and M. G. Bawendi, *Angewandte Chemie International Edition*, 1999, **38**, 1788-1791.
63. V. Mazumder and S. Sun, *Journal of the American Chemical Society*, 2009, **131**, 4588-4589.
64. Y.-H. Shih, G. V. Sagar and S. D. Lin, *The Journal of Physical Chemistry C*, 2007, **112**, 123-130.
65. M. Nesselberger, M. Roefzaad, R. Fayçal Hamou, P. Ulrich Biedermann, F. F. Schweinberger, S. Kunz, K. Schloegl, G. K. H. Wiberg, S. Ashton, U. Heiz, K. J. J. Mayrhofer and M. Arenz, *Nat Mater*, 2013, **12**, 919-924.
66. O. Otelaja, D.-H. Ha, T. Ly, H. Zhang and R. D. Robinson, *ACS Appl Mater Interfaces*, 2014, **6**, 18911.
67. N. M. Markovic, B. N. Grgur and P. N. Ross, *J Phys Chem B*, 1997, **101**, 5405-5413.
68. D. Strmcnik, D. Tripkovic, D. van der Vliet, V. Stamenkovic and N. M. Marković, *Electrochemistry Communications*, 2008, **10**, 1602-1605.
69. C. Ji and P. C. Searson, *The Journal of Physical Chemistry B*, 2003, **107**, 4494-4499.
70. Y. Ding and J. Erlebacher, *Journal of the American Chemical Society*, 2003, **125**, 7772-7773.
71. Y. Liu, S. Bliznakov and N. Dimitrov, *Journal of Physical Chemistry C*, 2009, **113**, 12362-12372.
72. R. Li and K. Sieradzki, *Physical Review Letters*, 1992, **68**, 1168-1171.
73. R. Boggio, A. Carugati and S. Trasatti, *J Appl Electrochem*, 1987, **17**, 828-840.
74. E. B. Budevski, G. T. Staikov and W. J. Lorenz, *Electrochemical Phase Formation and Growth: An Introduction to the Initial Stages of Metal Deposition*, Wiley, 2008.
75. A. Minguzzi, F.-R. F. Fan, A. Vertova, S. Rondinini and A. J. Bard, *Chemical Science*, 2012, **3**, 217-229.
76. K. Márquez, G. Staikov and J. W. Schultze, *Electrochimica Acta*, 2003, **48**, 875-882.
77. M. Miranda-Hernández, M. Palomar-Pardavé, N. Batina and I. González, *Journal of Electroanalytical Chemistry*, 1998, **443**, 81-93.
78. S. Djokić, N. Nikolić, P. Živković, K. Popov and N. Djokić, *ECS Transactions*, 2011, **33**, 7-31.
79. D. Grujicic and B. Pesic, *Electrochimica Acta*, 2004, **49**, 4719-4732.
80. P. Comba and A. F. Sickmuller, *Inorg Chem*, 1997, **36**, 4500-4507.
81. E. Herrero, L. J. Buller and H. D. Abruña, *Chemical Reviews*, 2001, **101**, 1897-1930.
82. R. Vasilic and N. Dimitrov, *Electrochemical and Solid-State Letters*, 2005, **8**, C173.
83. H. T. Zhang, B. Hu, L. F. Sun, R. Hovden, F. W. Wise, D. A. Muller and R. D. Robinson, *Nano Letters*, 2011, **11**, 5356-5361.
84. N. M. Markovic, C. A. Lucas, V. Climent, V. Stamenkovic and P. N. Ross, *Surf Sci*, 2000, **465**, 103-114.

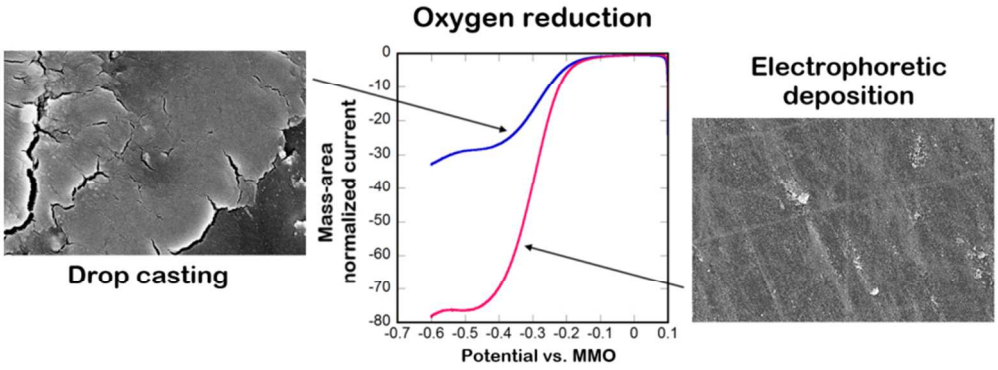

Electrophoretic deposition was found to improve the activity of cobalt oxide nanoparticulate thin films for oxygen reduction/evolution in spite of an apparent decrease in active surface area.
80x31mm (300 x 300 DPI)